Max-Planck-Institut für Meteorologie

REPORT No. 95

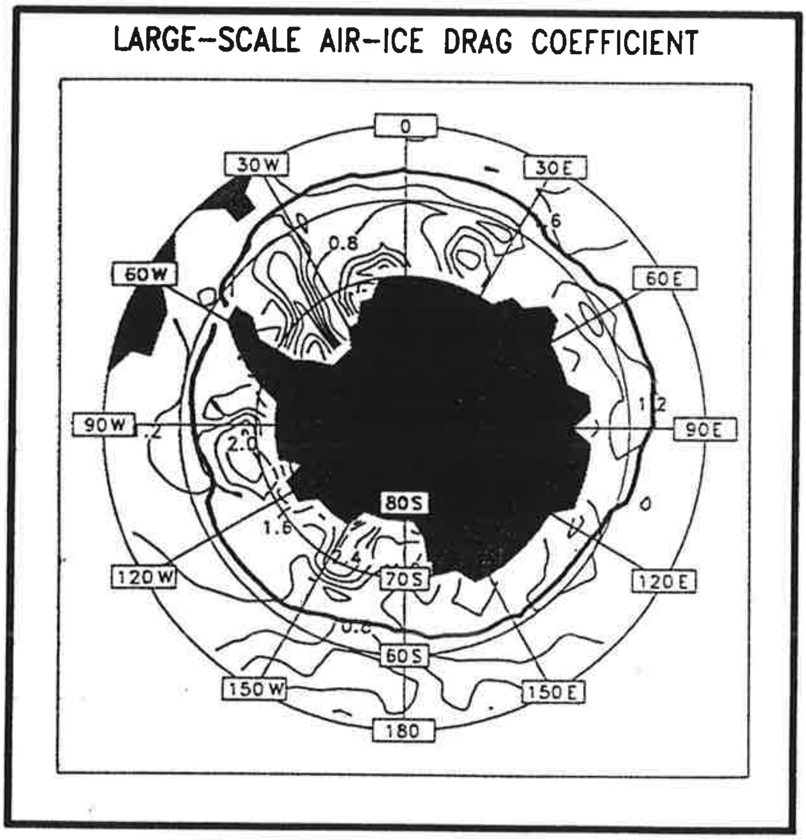

A NEW ATMOSPHERIC SURFACE-LAYER SCHEME FOR A LARGE-SCALE SEA-ICE MODEL

by

ACHIM STÖSSEL • MARTIN CLAUSSEN

HAMBURG, NOVEMBER 1992

AUTHORS:

Achim Stössel
Martin Claussen

Max-Planck-Institut
für Meteorologie

MAX-PLANCK-INSTITUT
FÜR METEOROLOGIE
BUNDESSTRASSE 55
D-2000 HAMBURG 13
F.R. GERMANY

Tel.: +49 (40) 4 11 73-0
Telex: 211092 mpime d
Telemail: MPI.METEOROLOGY
Telefax: +49 (40) 4 11 73-298

REPb 95

ISSN 0937-1060

A new Atmospheric Surface-Layer Scheme for a Large-Scale Sea-Ice Model

Achim Stössel and Martin Claussen
Max-Planck-Institut für Meteorologie
Bundesstr.55, 2000 Hamburg 13, Germany

Abstract

A large-scale sea-ice – oceanic mixed-layer model for the Southern Ocean is forced with daily atmospheric fields from operational numerical weather prediction analyses. The strength of the atmospheric forcing is modified by including atmospheric surface-layer physics, which is itself directly dependent on the instantaneous sea-ice condition provided by the sea-ice model.

In earlier applications, the atmospheric drag on sea ice was computed from the local momentum transfer over ice. In the present study, this is substituted by a large-scale momentum flux, which is a function of a large-scale Richardson number and a large-scale roughness length. The large-scale Richardson number is determined by the ice-concentration-weighted local turbulent heat fluxes and local friction velocities. The large-scale roughness length, on the other hand, depends on the local skin drags and on the form drag, where the latter is given as a function of the ice-plus-snow freeboard and the ice concentration, both provided by the sea-ice model. The thermodynamic part of the calculation is given by the local fluxes, which depend on the local stability of the atmospheric surface layer.

This physically more reasonable description of the dynamic forcing can lead to unstable stratification even in regions of high ice compactness, yielding larger stresses than the earlier parameterisation. The new parameterisation leads to improved model results in terms of ice-thickness distribution, ice velocities, mixed-layer depth and mean oceanic heat flux.

Introduction

Scientists engaged in coupled ocean - atmosphere general circulation model (GCM) experiments have generally recognised that the simulation results in high and mid-latitudes are highly dependent on the treatment of the sea-ice component (Meehl and Washington, 1990; Manabe et al., 1992; Cubasch et al., 1992). Results of coupled GCM experiments with increasing greenhouse-gas concentrations show a 50-100 % stronger warming over the polar regions of the northern hemisphere than the global mean (IPCC, 1990). This is primarily related to a wintertime increase of the atmospheric surface temperature over sea ice. While this is a remarkable and much quoted result, it should be noted that the treatment of the sea-ice component in such models is rather crude in comparison to the sea-ice models used for regional polar studies.

A physically more realistic description of the sea-ice component, specifically in terms of a viscous-plastic constitutive law for the ice dynamics, seems to lower the overall sensitivity of sea ice considerably. Furthermore, it leads to improved ice drift patterns and magnitudes, which modify the annual net freezing rate by more realistic representations of the divergence and convergence within the ice pack. The annual net freezing, on the other hand, is an important upper boundary condition for the ocean in modifying the density of the oceanic mixed layer and hence the thermohaline circulation. Additionally considering the insulation effect of snow on sea ice (representing another first order effect (Stössel et al., 1990)) in coupled GCMs, the greenhouse-warming impact in polar regions may alter substantially.

The other crucial part of the sea-ice treatment is the proper determination of the fluxes between the atmosphere, sea-ice and ocean components. In order to ensure this, it appears to be necessary to resolve more physical processes within the transition zones from one component to the other, i.e. to account for boundary-layer processes including sub-grid scale features due to surface heterogeneities.

This is a problem which ought to be addressed already in forced experiments. Questions concerning interactive and boundary-layer processes together with the specification of the appropriate forcing (coupling) interface are inherent and decisive for forced simulations, too.

In sea-ice regions the dominant factors controlling the strength of the forcing or coupling between atmosphere and sea ice originate from the extremely heterogeneous horizontal distribution of static stability within the atmospheric boundary layer and the atmospheric surface layer (ASL), and the variations in surface roughness due to variable ice and snow thicknesses, due to deformations in form of pressure ridges and due to variable ice coverage. These aspects are referred to in Stössel (1992) and Claussen (1991a).

Another aspect not very well accounted for so far is related to the large-scale application of the sea-ice component. Since sea-ice simulations on GCM scales are far from resolving ice floes, sea ice is treated as a continuum. However, options are provided to present a grid cell partially ice covered (expressed by the ice concentration or ice compactness), dividing the grid cell into two regions with totally different characteristics of the respective (local) atmospheric boundary layers. Furthermore, the local boundary layers merge to a mixture of their characteristics beyond a certain height above the surface (so-called blending height) depending on the specific distribution of the ice-covered and ice-free part within a grid cell.

In earlier sea-ice simulations (Stössel, 1992) the forcing level was established at some height above the surface in order to introduce modifications of the forcing based on atmospheric surface-layer physics. Specifying the atmospheric forcing above the blending height suggests the boundary-layer modifications of the dynamic forcing to be determined by "large-scale" or "effective" boundary-layer quantities. These are calculated as functions of the ice concentration, ice freeboard, snow thickness and the local surface-layer quantities, representing the main issue of this paper.

After some basic comments on the applied models and forcing fields in section 2, a detailed description of the large-scale modifications to the earlier atmospheric surface-layer formulation is given in section 3. The impact of these modifications on the results are presented in section 4, primarily as differences from the earlier studies.

2. Basic Models and Forcing Fields

The basic model consists of a dynamic-thermodynamic sea-ice model coupled to an oceanic mixed-layer model, both described in detail in Lemke et al.(1990). Snow is accounted for according to Owens and Lemke (1990). Atmospheric boundary-layer parameterisations were introduced by Stössel (1992). The earlier literature is referred to for the model formulations, since they are rather comprehensive and not critical for the present study.

As in the earlier studies, the region of interest is the entire Southern Ocean. Following Stössel (1992), the model grid is spherical with $\Delta\varphi = 2.5^{\circ}$ and $\Delta\lambda = 5^{\circ}$, the time step is one day and the integration time 6 years to achieve cyclostationarity with respect to the ice volume. The main atmospheric forcing variables consist of real-time daily mean temperature, humidity and winds at the 1000 hPa level from the global analyses of the European Center for Medium Range Weather Forecasts (ECMWF) (Trenberth and Olson, 1988). The surface pressure is derived from variables of the same data set. The reasons for using these essentially model generated data and the reconstruction of the actual forcing level are described in detail in Stössel (1991, 1992). For the 6-year integration, the first five years are run with the real-time forcing from the year 1985, while the sixth year is determined by the year 1986. All other forcing variables in terms of precipitation, cloudiness, geostrophic currents, and temperature and salinity at the base of the second oceanic layer (= 500 m depth) are also equivalent to the earlier specifications (see Stössel et al., 1990).

The equations of interest for the present study are those of the atmospheric surface-layer parameterisation and those related to the heterogeneous surface of a model grid cell. In the earlier applications it was assumed that the boundary layers develop separately (locally) over the ice-free and the ice-covered part of a grid cell. In the present study, this scheme is retained to calculate the local heat budgets, which largely determine the ice growth rates. Specifically, it is assumed that the turbulent heat fluxes are governed by the local stabilities of the respective ASLs. The motivation for this approach is given in Stössel (1992) and is summarised in the following.

Independent of which atmospheric forcing is used, there is only one forcing variable (e.g. air temperature) per grid cell available. This actually ought to be a blend of data sampled over the instantaneous (heterogeneous) sea-ice distribution in the grid cell area or, in case of an atmospheric GCM (AGCM) product, a result depending on the instantaneous boundary conditions of the AGCM. By raising the forcing level to the top of the ASL, the requirement for local atmospheric surface forcing variables (2 m or 10 m quantities) is relaxed, the local thermal forcing being determined via the local ASL properties.

The formulas describing the atmospheric surface layers were derived from Louis (1979). They are based on the Monin-Obukhov similarity theory, the Monin-Obukhov length being replaced by the Richardson number for the lowest atmospheric layer. The local Richardson numbers over the ice-covered ($_i$) and the ice-free ($_o$) parts yield

$$Ri_{i,o} = gz_a\left(\theta_a - \theta_{i,o} + 0.61\theta_a(q - q_{i,o})\right)/(\theta_a|\vec{V}_a|^2), \qquad (1)$$

where g : acceleration due to gravity,

z_a : height of the lowest atm. layer (= forcing level),

θ_a : pot. temperature of the lowest atmosphere layer,

θ_i : pot. temperature at ice-covered surface (= T_i),

θ_o : pot. temperature at ice-free surface (= T_o),

$T_{i,o}$: local surface temperatures,

q : specific humidity of lowest atmosphere layer,

$q_{i,o}$: specific humidities at the local surfaces,

$\vec{V}_a$: wind in the lowest atmosphere layer.

Here, the surface variables are determined by the local surface properties, e.g. T_i by the ice- or snow-surface temperature in the ice-covered part and T_o by the sea-surface temperature (≡ oceanic mixed-layer temperature T_{o1} in Stössel, 1992) in the ice-free part (= freezing point, when ice occurs within a grid cell).

In the present application, z_a = 30 m, unless the surface pressure exceeds ≈ 1004 hPa, i.e. the 1000 hPa level lies above 30 m. In this case, z_a increases together with the 1000 hPa level (Stössel, 1991).

The local friction velocities ($u_{*i,o}$) are defined from the vertical eddy fluxes of momentum:

$$(\overline{w'u'})_{i,o} \equiv u^2_{*i,o} = \left(\frac{\kappa}{\ln(z_a/z_{0i,o})}|\vec{V}_a|\right)^2 F_{mi,o}, \qquad (2)$$

where κ : von Karman constant,

$z_{0i,o}$: local roughness lengths,

$F_{mi,o}$: stability functions for local momentum fluxes.

Following Stössel (1992), the local roughness length over ice is specified as $z_{0i} = 1\cdot10^{-3}$m. The roughness over the ice-free part is determined by the local wind-generated waves, implicitly formulated by $z_{0o} = Cu^2_{*o}/g$, where C = 0.032 is the Charnock constant.

The corresponding scaling temperatures ($\theta_{*i,o}$) are assumed to be related to the vertical eddy fluxes of sensible heat:

$$- \left(\overline{w'\theta'}\right)_{i,o} \equiv (u_*\theta_*)_{i,o} = - \frac{Q_{sei,o}}{\rho_a c_{pa}} = \frac{\kappa^2 |\vec{V}_a| (\theta_a - \theta_{i,o}) F_{hi,o}}{0.74 \ln^2 (z_a / z_{0i,o})}, \qquad (3)$$

where $Q_{sei,o}$: local sensible heat fluxes,

ρ_a : air density,

c_{pa} : specific heat of air at constant pressure,

$F_{hi,o}$: stab. functions for local turbulent heat fluxes.

The (local) latent heat fluxes ($Q_{lai,o}$) are given by analogous formulas with q and $q_{i,o}$.

After a slight modification according to Claussen (1991a), the stability functions combine as follows:

$$F_{m,h} = \left(\frac{1}{(1 + 2 \cdot 4.7 Ri)^2} \right) \delta_{jk} + \left(1 - \frac{9.4 Ri}{1 + c_{m,h} |Ri|^{0.5}} \right) (1 - \delta_{jk}), \qquad (4)$$

where δ is the Kronecker symbol and $j = k$, if $Ri \geq 0$,

with $$c_{m,h} = (7.4, 5.3) \left(\frac{\kappa}{\ln(z_a / z_0)} \right)^2 9.4 \sqrt{\frac{z_a}{z_0}} \ .$$

For neutral and convective stratifications these formulas follow from analytical adaptations to the functions of Businger et al. (1971). In the case of highly stable stratifications, the expression for $F_{m,h}$ follows from an asymptotic approach toward zero for increasing Richardson numbers (Louis, 1979).

3. Modifications for large-scale applications

In earlier applications (Stössel, 1992) the momentum transfer from the atmosphere to the ice was determined by local properties. However, observations and simulations (e.g. Hanssen-Bauer and Gjessing, 1988; Andreas et al., 1984; Overland and Davidson, 1992; Claussen, 1991a; Simmonds and Budd, 1991; Worby and Allison, 1991; Stössel, 1992) suggest this momentum transfer to be determined by aggregated, grid-cell averaged quantities. For large-scale modelling it is often proposed to consider sub-grid scale effects due to heterogeneous compositions at the surface by weighting the local properties linearly with the surface composition. Observations, however, imply that certain surface features, e.g. leads in the case of sea ice, may dominate the large-scale characteristics, even when their fraction is rather small (Claussen 1991b). This non-linear behaviour is accounted for in the present study by a blend of the local ASL properties. The translation of the sub-grid scale properties to the large-scale quantities is described in the following.

First, it is necessary to introduce a measure for the surface roughness in terms of an "effective" or "large-scale" roughness length. In sea-ice areas with ice compactnesses lower than 100 %, the effective roughness length is determined by the freeboard of the (level) ice floes (including snow), by the size of the floes, by pressure ridges, by the local skin frictions and by the sea-surface roughness of the ice-free parts (waves).

The (effective) ice (plus snow) freeboard is given by

$$h_f = \left((1 - \rho_i/\rho_w)(h_i + h_s\rho_s/\rho_i) - h_s\rho_s/\rho_i + h_s\right) / N_i \, , \tag{5}$$

where ρ_i : density of sea ice,

ρ_w : density of water,

ρ_s : density of snow,

h_i : mean (grid cell averaged) ice thickness,

h_s : mean snow thickness,

N_i : ice coverage per grid cell.

In order to avoid exaggerated freeboards at locations where snow has accumulated to a few meters, a snow to ice conversion is introduced closely following Leppäranta (1983) and Stössel (1985). Instead of creating a new aggregate in form of snow ice, however, snow is directly converted into ice whenever the weight of the snow exceeds the buoyancy of the ice-plus-snow column to an extent that the snow submerges below the water line. The draft of the ice-plus-snow column is given by:

$$h_d = (\rho_s h_s + \rho_i h_i) / \rho_w \quad . \tag{6}$$

Whenever $h_d > h_i$, h_i is set equal to h_d and the snow thickness is reduced by

$$\Delta h_s = (h_i - h_d)\, \rho_i / \rho_s \quad . \tag{7}$$

Additionally, it is necessary to know the horizontal scale of roughness variations, $\hat{L}$. Over sea ice, $\hat{L} = L_i + L_o$, where L_i is the floe size and L_o the lead size, both considered parallel to the upwind direction. Since these quantities are not provided by the sea-ice model, the average floe size is assumed to be given as a function of the effective ice thickness ($\tilde{h}_i = h_i / N_i$), e.g. $L_i = \tilde{h}_i \cdot 100$. As will be shown later, this estimation can be related to the "relative length β" ($\beta = L_i / h_f$) introduced by Hanssen-Bauer and Gjessing (1988).

Because the sea-ice model does not provide any information about the height and frequency of pressure ridges, its roughness contributions are neglected. This is not considered to be critical, because there is some compensation due to the addition of snow, which in the present formulation is added as a rigid body on top of the ice (Eq. 5). Since snow usually smoothens at the windward edges, its contribution to the surface roughness appears to be somewhat overestimated.

After the surface roughness conditions have been introduced, the derivation of the large-scale ASL quantities is described in the following.

In order to express the effective wind stress (also called total wind drag) $\tilde{\tau}_a$ over a heterogeneous area of sea ice, the drag partition theory is used (Arya, 1975):

$$\tilde{\tau}_a = \langle \tau_S \rangle + \tau_F, \tag{8}$$

where $\langle \tau_S \rangle$: mean skin drag ($= N_i \tau_{Si} + (1-N_i)\tau_{So}$),

τ_{Si} : local skin drag over ice-covered part,

τ_{So} : local (undisturbed) skin drag over ice-free part,

τ_F : form drag due to floe edges.

A detailed discussion of the drag partition theory is found in Marshall (1971) together with its evaluation in wind-tunnel experiments.

In turbulent flow over rough surfaces, the division between skin and form drag is somewhat arbitrary. In the present application, the skin drag is considered to be that portion of the drag which is associated with roughness elements with dimensions of the order of a few centimeters or less. The effect of these small elements on the surface-layer flow is determined by the local roughness lengths of ice (z_{0i}) and of water (z_{0o}), respectively. The influence of larger roughness elements are represented by the form drag, which is part of the parameterisation of the effective roughness length.

In accordance with Arya (1975), it is assumed that wakes, which originate at downwind obstacles, blend at a height z_b such that for heights $z_a \ll z_b$ the flow is in equilibrium with the local surface, whereas for $z_a \gg z_b$ single wakes are not supposed to be identified individually, i.e. the flow just 'feels' a rougher surface. For heights $z_a \ll z_b$, and not too close to the obstacles, the wind profile can be parameterised by the local roughness lengths and local friction velocities. For $z_a \gg z_b$, on the other hand, the wind profile is a function of an effective roughness length $\tilde{z}_0$ and an effective friction velocity $\tilde{u}_*$. At the blending height z_b, both conditions are approximately met. Thus, the ratio of the total aerodynamic drag to the (undisturbed) skin drag over open water yields

$$\frac{\tilde{\tau}_a}{\tau_{So}} = \left(\frac{\ln(z_b/z_{0o})}{\ln(z_b/\tilde{z}_0)}\right)^2, \tag{9}$$

so that for the effective roughness length $\tilde{z}_0$:

$$\ln(\tilde{z}_0/z_{0o}) = \ln(z_b/z_{0o})\left(1 - (\tilde{\tau}_a/\tau_{So})^{-0.5}\right) . \tag{10}$$

In order to compute the effective roughness length, the mean skin drag ($\langle\tau_S\rangle$) and the form drag (τ_F) have to be known. The ratio of the form drag to the open-water skin drag is assumed to be given by:

$$\frac{\tau_F}{\tau_{So}} = \frac{c_d h_f}{2\hat{L}} \left(\frac{s}{\kappa} \ln(h_f/(e z_{0o})) \right)^2 , \tag{11}$$

where $s = (1 - \exp(-0.18 L_o/h_f)$,

$e = \exp(1)$,

and c_d is the 'roughness-element' drag coefficient introduced by Marshall (1971) which is set equal to 1 here, following Hanssen-Bauer and Gjessing (1988). According to the same authors, s is a factor which accounts for sheltering effects at floe edges.

With respect to the estimation $L_i = \tilde{h}_i \cdot 100$ given earlier, the approximation $h_f \approx 0.1 \cdot \tilde{h}_i$ in case of zero snow cover yields $\beta \approx 1000$. Accounting for snow, however, with h_s being on the average some 10 % of h_i, β yields a value of approximately 500. Quantifying this value in terms of τ_F/τ_{So} as a function of ice compactness (Hanssen-Bauer and Gjessing, 1988), the maximum form drag is achieved at $N_i \approx 90$ %. This value is in good agreement with observations across the Southern Ocean ice edge (Andreas et al., 1984).

The ratio of the mean skin drag to the open-water skin drag is estimated by assuming that the large-scale turbulent fluxes merge at sufficiently large heights above the ground. It is suggested that this height is roughly as large as the blending height z_b. Furthermore, attenuation of skin drag on narrow leads due to wind reduction upwind and downwind of ice-floe edges is neglected. It was shown by Hanssen-Bauer and Gjessing (1988) that this effect is small for $\beta \geq 500$ (its sensitivity will be evaluated in section 4.3). Hence

$$\frac{\langle \tau_S \rangle}{\tau_{So}} = \left(\frac{\ln(z_b/z_{0o})}{\ln(z_b/\langle z_0 \rangle)} \right)^2 , \tag{12}$$

where $\langle z_0 \rangle$ is the aggregated roughness length of z_{0i} and z_{0o}. As shown in Claussen (1991a), $\langle z_0 \rangle$ can be derived from

$$\ln \langle z_0 \rangle = N_i \ln z_{0i} + (1 - N_i) \ln z_{0o}, \tag{13}$$

providing a reasonable estimate.

The blending height is supposed to vary with the average distance between ice-floe edges. The dispersion of wakes generated at the edges is presumably governed by the same processes, leading to the development of internal boundary layers downstream of a step change in surface roughness. Claussen (1991b) argues that $\ln(z_b/\langle z_0\rangle)z_b/\hat{L} \sim 0.35$. Here

$$z_b = \langle z_0\rangle^{0.2}(\hat{L}/2)^{0.8} \qquad (14)$$

is used as a simple, but convenient approximation. Since $z_b \gg \langle z_0\rangle$, a precise evaluation of z_b is not necessary. An order of magnitude estimate turns out to yield sufficiently accurate large-scale momentum fluxes.

With respect to the turbulent heat fluxes, empirical data discussed in Beljaars (1982) and Beljaars and Holtslag (1991) support the conjecture that over a terrain with steep roughness elements, they are not directly affected by the form drag of such elements. Therefore, Claussen (1992) suggests evaluating only large-scale momentum fluxes from the large-scale roughness length, whereas turbulent heat fluxes should be estimated from local roughness lengths. Thus, it is consistent with Stössel (1992) to compute the turbulent heat fluxes locally over each surface type, with the forcing being specified at approximately the level of the blending height (Claussen, 1991b). Since the local roughness lengths of ice and water do not differ strongly, computation of heat fluxes at any level z_a within the surface layer seems to be a fair approximation, provided that z_a and z_b are of the same order of magnitude (Claussen, 1991a). Therefore, the turbulent heat fluxes are calculated locally using Eq.(3).

Local momentum fluxes (due to skin drag only) are obtained in the same manner. Finally, local momentum and turbulent heat fluxes are averaged by weighting with the ice compactness:

$$\langle Q_{se,la}\rangle = N_i Q_{se,lai} + (1 - N_i)\, Q_{se,lao} \qquad (15)$$

and

$$\langle u_*^2\rangle = N_i u_{*_i}^2 + (1 - N_i)\, u_{*_o}^2 \,. \qquad (16)$$

From these averaged (local) fluxes, an average Monin-Obukhov length is determined:

$$\langle L\rangle = \frac{-T_a \langle u_*\rangle^3 \rho_a c_{pa}}{\kappa g(\langle Q_{se}\rangle + 0.61 T_a c_{pa} \langle Q_{la}\rangle / L_v)} , \tag{17}$$

where L_v is the latent heat of evaporation. $\langle L\rangle$ is subsequently transferred into a bulk Richardson number by means of averaged stability functions:

$$\langle Ri\rangle = \frac{z_a \langle f_h\rangle}{\langle f_m\rangle^2 \langle L\rangle} , \tag{18}$$

where $\langle f_{m,h}\rangle = f(z_a/\langle L\rangle)$ follow from the vertical integration of the functions of Businger et al. (1971). This Richardson number of the averaged quantities ($\equiv$ large-scale Richardson number $\tilde{Ri}$) is used to evaluate the large-scale stability function for momentum transfer (substituting Ri and z_0 by the corresponding large-scale quantities in Eqs.(4)), which enters the formula for the large-scale friction velocity:

$$\tilde{u}_*^2 \equiv \left(\frac{\kappa}{\ln(z_a/\tilde{z}_0)} |\vec{V}_a| \right)^2 \tilde{F}_m(\tilde{Ri}) . \tag{19}$$

This friction velocity determines the effective drag coefficient ($\tilde{C}_d = (\tilde{u}_*/|\vec{V}_a|)^2$), which finally modifies the stress between atmosphere and sea ice ($\tilde{\tau}_a$).

4. Results

4.1 Major Impact

The major impact with the above modifications of the ASL parameterisation for the dynamic forcing of the sea-ice – oceanic mixed-layer model (Stössel, 1992) is expected to occur over sea ice with ice compactness between 90 and 99 %. This happens to be the dominant type of Antarctic sea-ice distribution in fall and winter (April to October). Thus, the analysis will focus on one winter situation (August 28, 1986). The impact of the new parameterisation will be represented largely as difference contours relating to the earlier results.

The absolute value in terms of ice compactness (Fig.1) can be verified against corresponding products derived from the earlier simulations with ASL parameterisation and observations (Figs.10.c and 11.c in Stössel, 1992). Compared to the earlier results, there appears to be a tendency toward slightly reduced ice concentrations in the interior ice pack and toward a higher zonal variability of the ice edge. Otherwise, the results are almost identical in terms of ice extent and width of the marginal ice zone (MIZ).

The final variable modifying the dynamic forcing of the sea-ice model is the large-scale drag coefficient. The areal distribution of its absolute value is shown in Fig.2. The most striking feature is the huge spatial variability of $\tilde{C}_d$, ranging from $0.1 \cdot 10^{-3}$ up to $3.6 \cdot 10^{-3}$. It reflects the synoptic-scale variability. At that time of the year, most regions are covered by highly compact sea ice, as can be identified from Fig.1. Nevertheless, while the locally determined drag over ice is rather low, the large-scale quantities provide a substantial drag.

This is emphasized in Fig.3 , where the difference in the magnitude of the drag coefficient compared to the earlier treatment is shown. A comparison with Fig.2 reveals that the patterns and magnitudes are similar, indicating that the former (local) drag coefficient over ice was rather small. This was due to the generally highly stable stratification over the winter ice pack, where the outgoing longwave radiation is the main contributor for decreasing the ice (or snow) surface temperature below the ambient air temperature.

As a consequence of using the large-scale drag coefficient instead of the locally determined one for the dynamic forcing of the sea-ice model, daily ice velocities encounter regionally (and temporarily) a substantial increase of up to 15 cm/s (Fig.4).

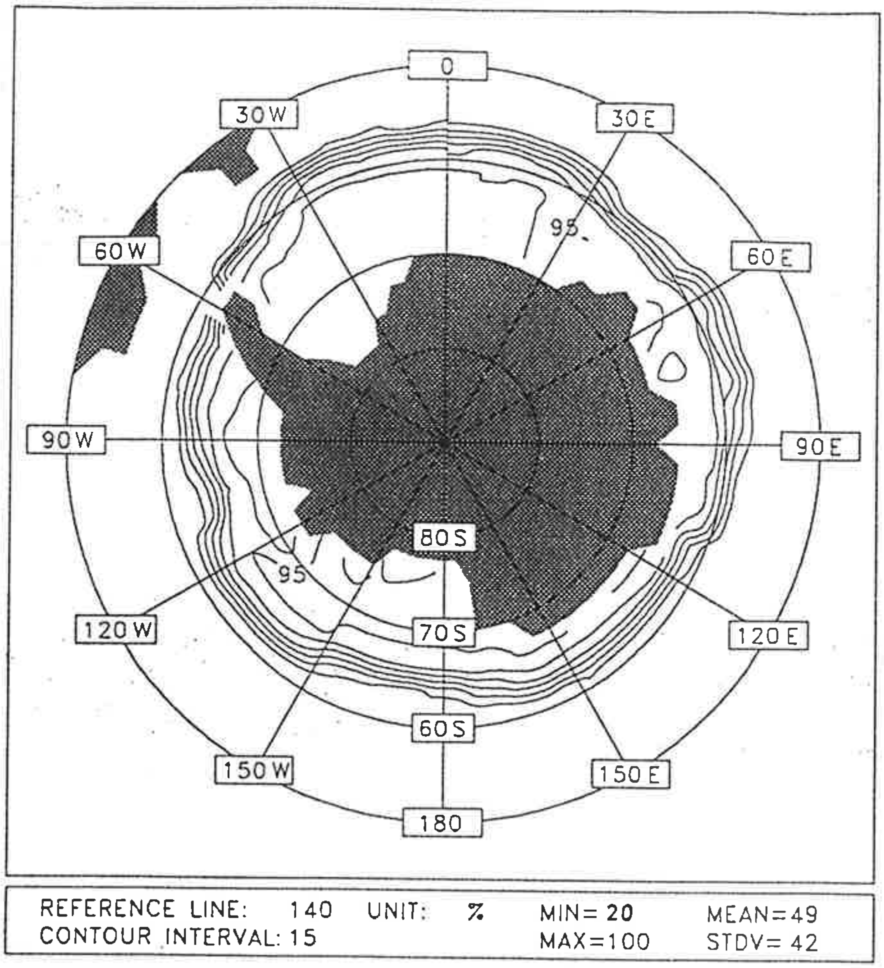

Fig. 1: Areal contours of ice concentration for an instantaneous wintertime situation (August 28, 1986) simulated with the dynamic forcing from the atmosphere modified with large-scale ASL quantities. The minimum contour line (N_i = 20%) is regarded as the ice edge and superimposed as a thick full line in the following figures.

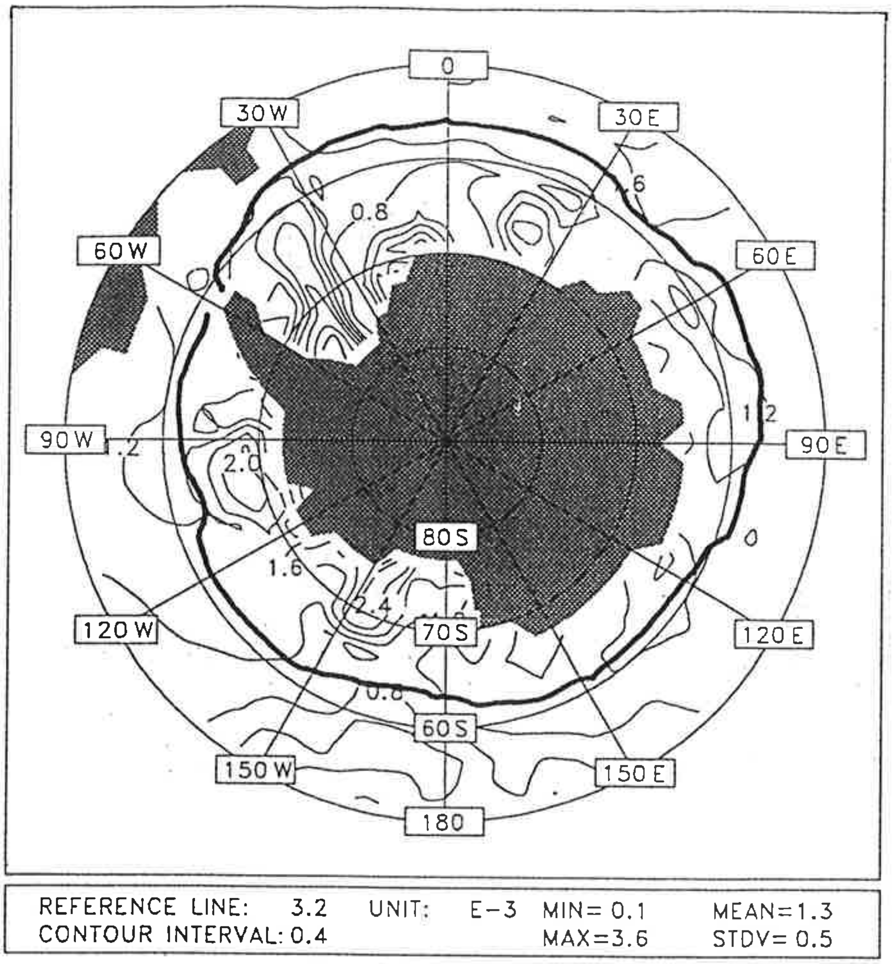

Fig. 2: Large-scale air-ice drag coefficient; otherwise as Fig. 1.

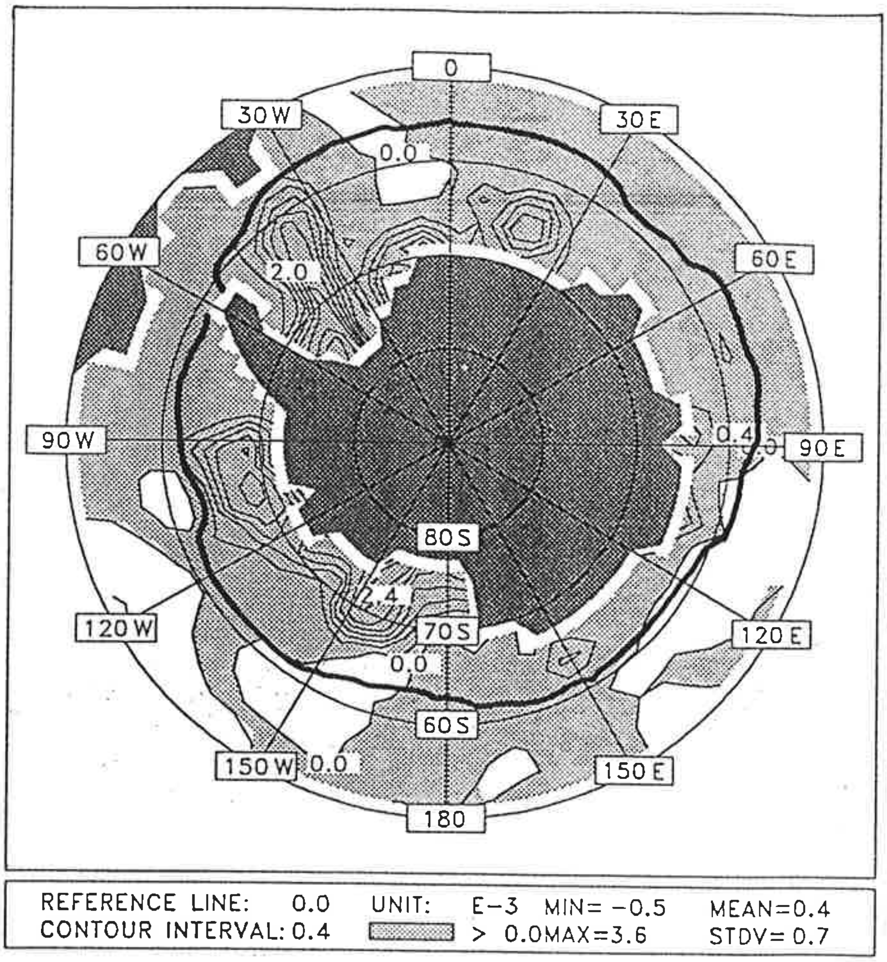

Fig. 3: Large-scale minus local air-ice drag coefficient, the latter simulated with the dynamic forcing modified by local ASL quantities; otherwise as Fig. 1.

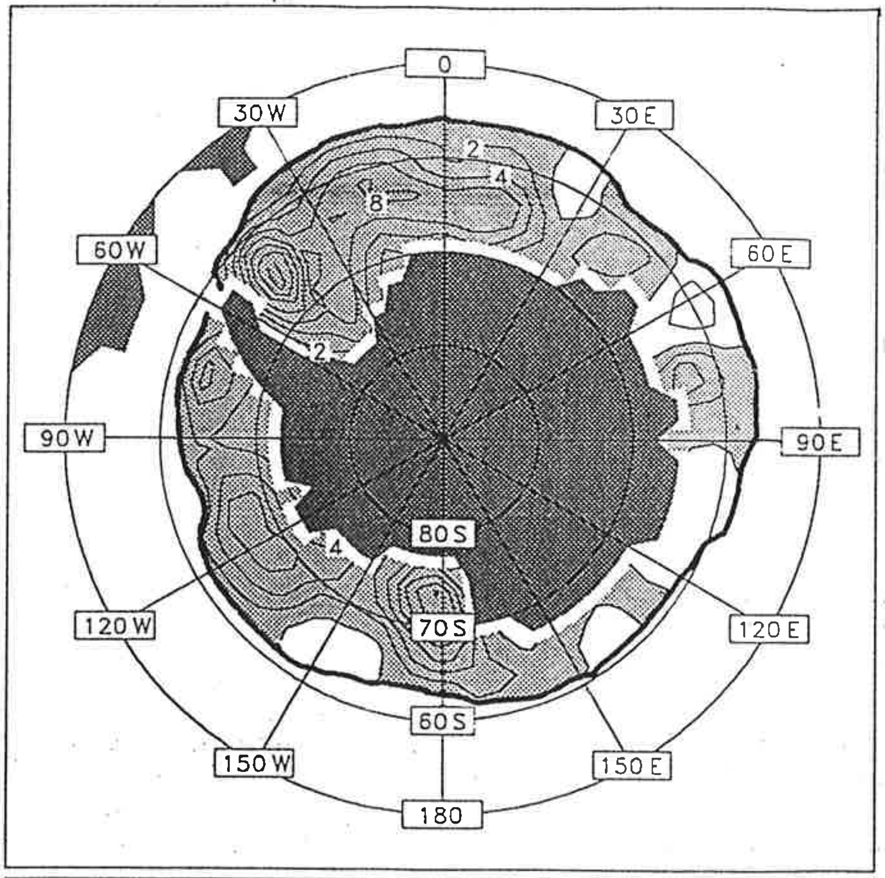

REFERENCE LINE: 0	UNIT:	cm/s	MIN= −3	MEAN=2	
CONTOUR INTERVAL: 2		> 0	MAX=15	STDV= 3	

Fig. 4: Ice-velocity differences with dynamic forcing derived from large-scale minus local quantities; otherwise as Fig. 1.

Except for locations in the Indian Ocean sector and in regions of lower ice concentrations along $\lambda = 150^{\circ}W$, all velocities are increased. The latter also holds for ice-velocity differences averaged over three months from June to August (Fig.5), except for the region between Antarctica and South America. Significant differences of mean ice velocities (up to 6 cm/s) are computed in central and offshore regions of the Weddell and Ross Seas.

The impact of the general increase of the ice-drift magnitude on the ice-thickness distribution is presented in Fig.6. Ice thicknesses in convergent regions are increased by up to one meter, with decreases of the same magnitude in divergent regions. Overall, the pattern yields a more dynamic character than before, leading regionally to closer agreement with observations, as far as they are available in terms of ice thickness (Wadhams et al., 1987; Lange and Eicken, 1991; Gow et al., 1987).

Due to the decrease of ice thickness in divergent ice-drift areas, the possibility for new-ice growth is enhanced, leading to more brine rejection followed by a stronger oceanic convection and a subsequent deepening of the oceanic mixed layer (Fig.7), especially in regions with offshore ice drift in the southern Weddell and Ross Seas. Accordingly, the vertical oceanic (entrainment) heat flux (not shown) is increased on the average by 1 - 2 W/m^2, leading to closer agreement with observations (Martinson, 1990; Gordon and Huber, 1990).

4.2 Analysis

The reasons for the above results are analysed in the following. In the present formulation the drag coefficient is determined by the (large-scale) roughness length and the (large-scale) stability of the ASL. The large-scale roughness length is shown as difference from the one used in the earlier formulation (Fig.8) to determine the dynamic forcing of the ice (Stössel, 1992). It was the local roughness length over ice which

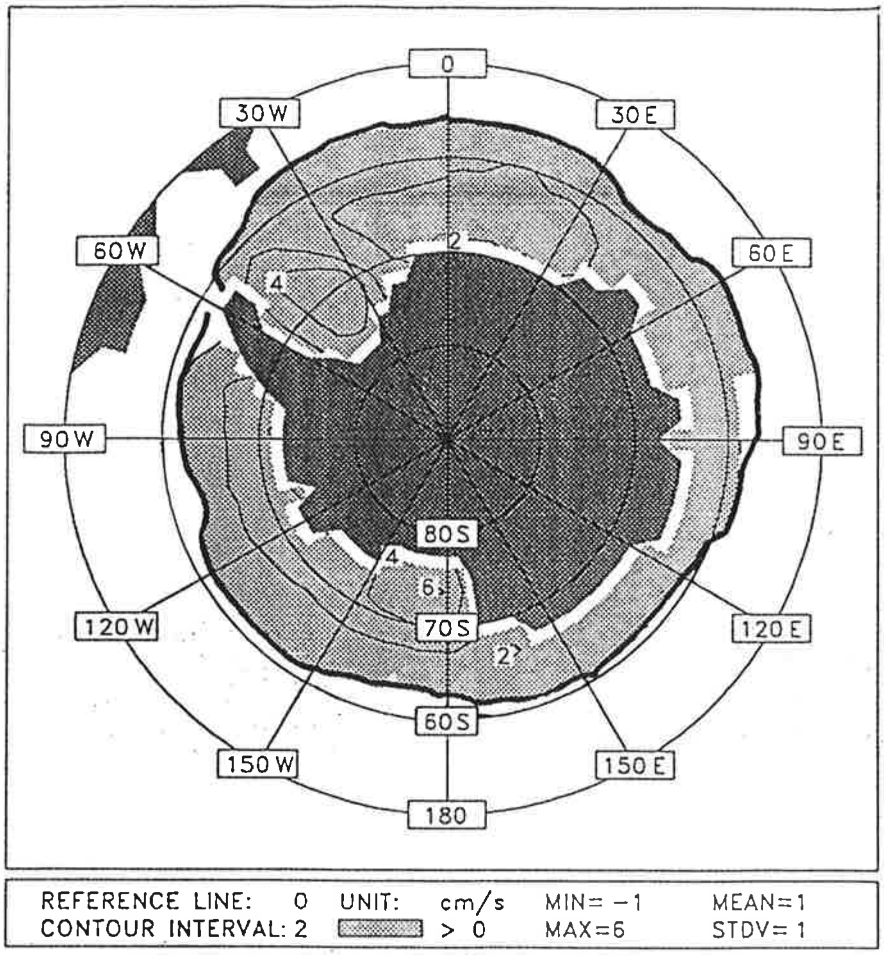

Fig.5: Quarterly (June, July, August) mean ice-velocity differences; otherwise as Fig.4.

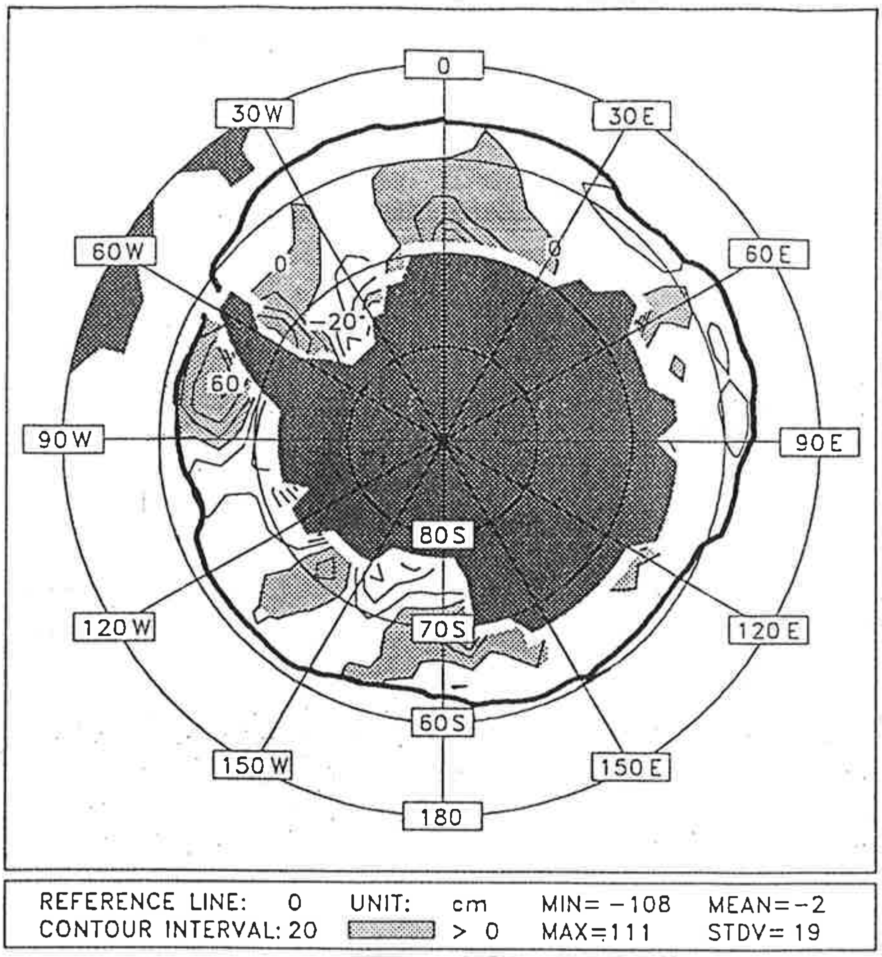

Fig.6: Ice-thickness differences; otherwise as Fig.4.

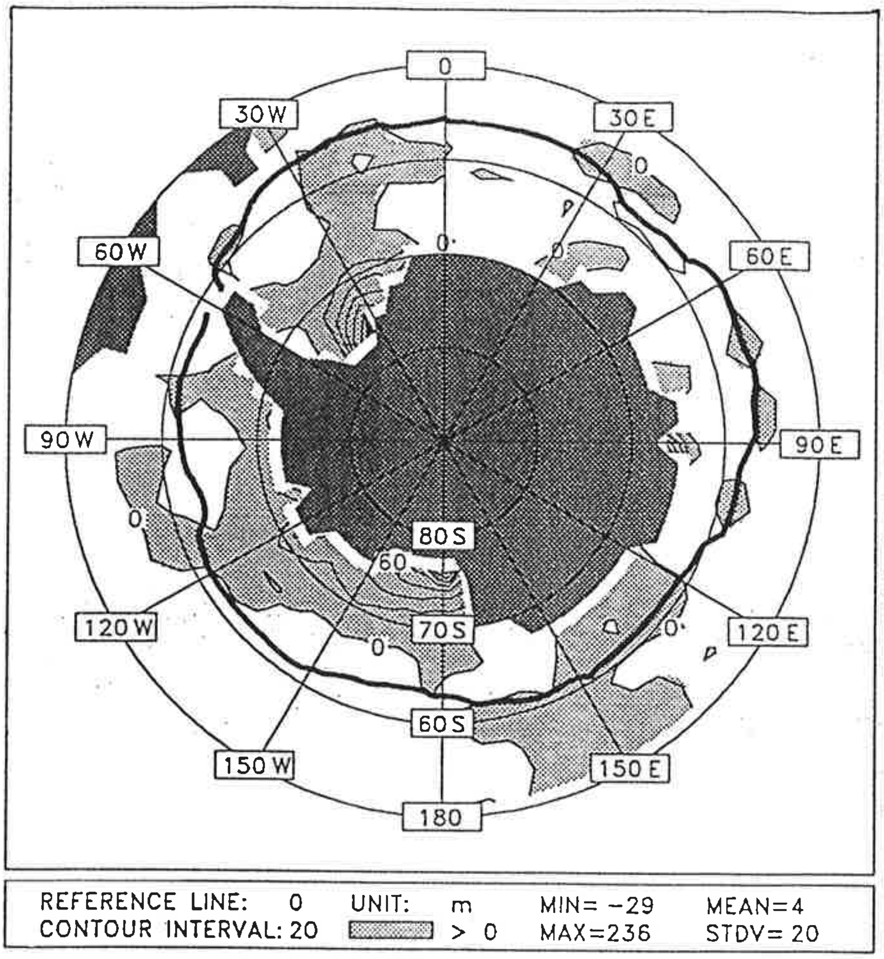

Fig. 7: Differences in oceanic mixed-layer depth; otherwise as Fig. 4.

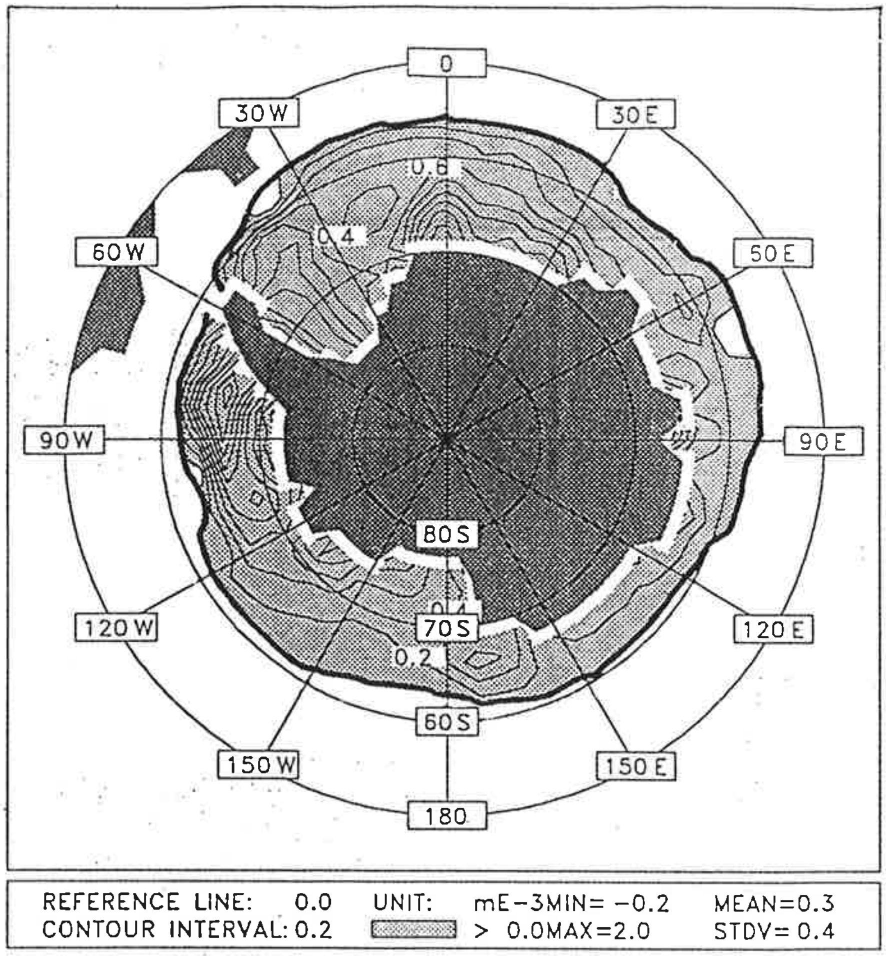

Fig. 8: Differences in large-scale roughness length; otherwise as Fig. 4.

was specified to be constant with $z_{0i}= 1\cdot10^{-3}$m. As can be identified from Fig.8, an overall increase is encountered, which locally (and temporarily) may exceed a factor of three. Since the most cumbersome quantity in the present scheme is the fetch over the ice floes and the leads, it is worthwhile to investigate the sensitivity of the large-scale roughness length to variations of those quantities. This is done by specifying constant values for L_i, ranging from 20 m to 2000 m. The most prominent differences between the upper and the lower case occur in terms of the large-scale roughness length ($\tilde{z}_0$) and, of course, the blending height (z_b; see Eq.(14)). While $\tilde{z}_0$ increases at the MIZ at the lower margin of L_i when compared with the standard prescription (not shown), it adopts almost the local value z_{0i} at the higher margin. Together with the fact that all other variables, especially $\tilde{C}_d$, do not vary significantly ($\tilde{C}_d$ at most 10 %), this implies that the varying large-scale roughness length has only a minor impact on the drag increase, if this is assumed to be determined by the floe size.

More dramatic changes occur when the freeboard of the ice-plus-snow column is increased, e.g. by one meter. Then the large-scale roughness length experiences an increase of up to one order of magnitude, and the large-scale drag coefficient correspondingly by a factor of up to two. Relating such exaggerated freeboards to observed features, one could associate them with heavily ridged ice floes. However, since such features are observed only occasionally in the Southern Ocean region (Lange and Eicken, 1991), it is not worthwhile to consider them in the present large-scale simulation. In the Arctic ice pack, on the other hand, higher pressure ridges and more hummocked ice are observed, which may lead to a stronger contribution to the large-scale roughness length (Overland, 1985).

The remaining candidate for the drag increase appears to be the large-scale stability of the ASL, illustrated in Fig.9 by the sign of the large-scale Richardson number, which distinguishes

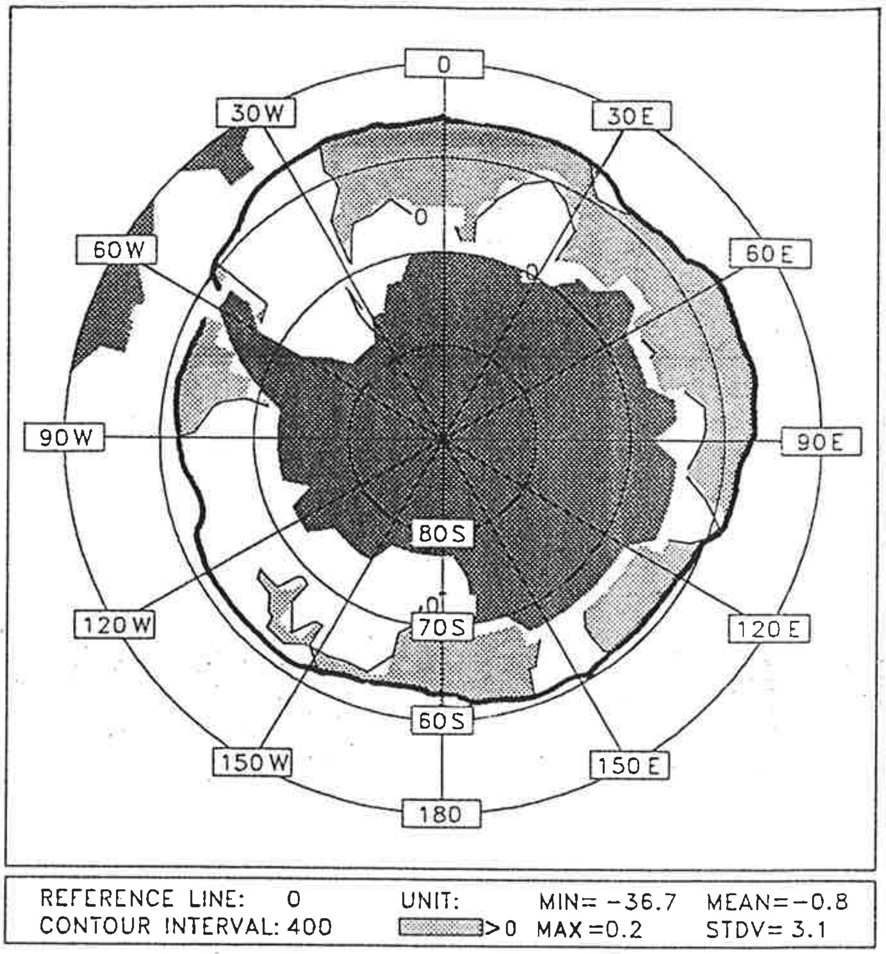

Fig. 9: Large-scale Richardson number; otherwise as Fig. 1.

between areas of stable (positive = shaded) and unstable (negative) stratifications. A high correlation of this pattern with the pattern of the large-scale drag coefficient is obvious (Fig.2).

4.3 Assessment

Immediately, the question arises whether the results are reasonable and represent an improvement. In terms of the ice drift and the ice-thickness distribution, the results seem to be more realistic than the earlier ones, judging by the sparse in-situ observations available. However, similar results could presumably also be achieved by changing the empirical parameters of the sea-ice model or by changing the ice-ocean drag (Stössel et al., 1990; Stössel, 1992). Thus, it is necessary to verify the individual ASL quantities, preferably by observations.

However, there is an inherent difficulty in deriving large-scale quantities from local observations. Hanssen-Bauer and Gjessing (1988) collected such data from two soundings over the Fram Strait ice pack with an ice compactness of 60 %, neutral stratification, a wind velocity of about 5 m/s, a mean freeboard of 0.4 m and a mean floe size of 20 m. Except for the observed large-scale roughness length, which differs by about one order of magnitude from our computations, our results for corresponding situations (exept for L_i) are similar. For the large-scale roughness length, the same order of magnitude as measured by Hanssen-Bauer and Gjessing (1988) is achieved when L_i is specified as 20 m and the extended formulation of the skin drag for $\beta < 500$ (Eq.(24) in Hanssen-Bauer and Gjessing, 1988) is used (Fig.10). Corresponding values occur in regions of lower ice compactness (which can be identified by more diffuse ice edges in Fig.1), especially in the Bellingshausen Sea, the Indian Ocean sector and the Scotia Sea, i.e. similar conditions to those during the measuring campaign of Hanssen-Bauer and Gjessing (1988). In

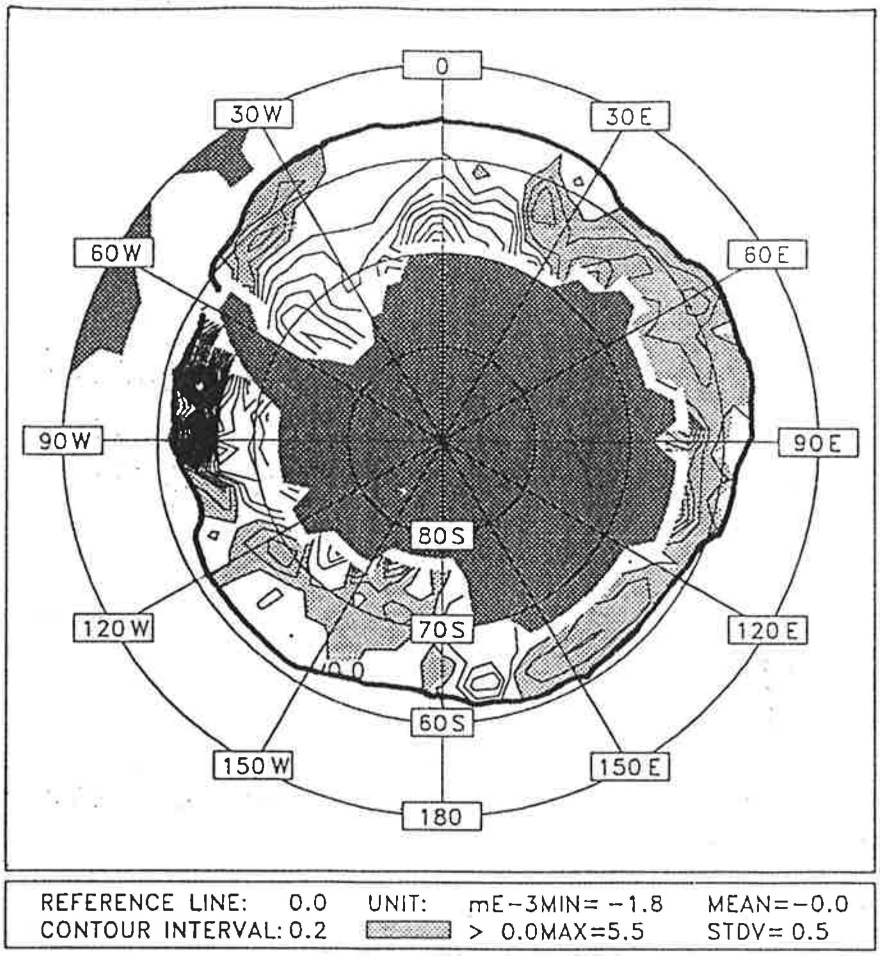

Fig. 10: Differences in large-scale roughness length of large-scale ASL modification with L_i = 20 m and extended skin drag formulation, minus standard large-scale ASL modification; otherwise as Fig. 1.

summer, $\tilde{z}_0$ agrees still more closely with the measured values of the above reference, which themselves are in fact samples of summer conditions.

The most decisive variable of the large-scale parameterisation is the large-scale drag coefficient. The range of the computed values ($0.1 \cdot 10^{-3}$ - $3.6 \cdot 10^{-3}$, see Fig.2) coincides with corresponding observed values (Andreas et al., 1984; Overland, 1985). While $\tilde{C}_d$ in Fig.2 represents primarily the 30 m value, the one usually referred to in the literature is the 10 m value, which is generally about 20 - 30 % higher. The upper and lower values of the large-scale drag coefficient are always correlated to highly unstable and highly stable stratifications in the ASL. The minimum of $0.1 \cdot 10^{-3}$ corresponds to a computed stability close to the critical Richardson number of 0.21, associated with low to moderate winds and very high ice compactnesses. This is within the same order of magnitude as derived from measurements (McBean, 1986) and agrees with the empirical derivation of the stable drag coefficient from the neutral one via z_a/L introduced by Banke et al. (1980). Adjusting measurements from low level flights over the central Arctic in winter (Walter and Overland, 1991) to ASL quantities, similar figures can be obtained.

The most prominent result is that the large-scale stratification may become unstable even in cases where the contribution of leads is as low as 3 %. It is known that in fall and wintertime even a small fraction of leads within the ice pack exerts a considerable impact on the overall heat balance (Maykut, 1986; Overland and Guest, 1991; Worby and Allison, 1991). If the leads are favourably distributed, the strong turbulence in the lead area of unstable stratification may even dominate the large-scale stratification by acting counter to the averaged positive vertical gradient of potential temperature (Claussen, 1991b). It remains to be verified, however, whether this is true for a small fraction of randomly distributed leads within the ice pack. Recent near-surface ($\approx$ 30 m) airborne measurements over Arctic sea ice in fall (Hartmann et al., 1992), covering a track from ice-free waters via the MIZ to areas of compact sea ice, indicate a high variability of the momentum fluxes. A corresponding variability in the sign of the turbulent heat fluxes suggests that the momentum fluxes are dominated by thermodynamic effects. Another means for deriving large-scale stratification may be provided by the satellite-borne TIROS-N Operational Vertical Sounder (TOVS), as the surface-temperature retrieval was recently improved (Francis, 1992).

A detailed analysis of such data together with their translation to stability in the ASL might give some support for the present results. It must be emphasized, however, that a large-scale Richardson number is certainly not a quantity which can directly be derived from measurements. In that sense it should be considered more as an artificial quantity introduced in order to cope with the different scales involved.

5. Conclusions

An attempt has been made to modify the dynamic atmospheric forcing for a large-scale sea-ice – oceanic mixed-layer model by deriving large-scale ASL and roughness parameters from local, sub-grid scale quantities. An essential assumption for this derivation is the specification of the forcing at a level of the order of the blending height.

The final variable modifying the dynamic forcing is the large-scale drag coefficient, which appeared to be highly variable on the synoptic scale. Enhanced drag was primarily associated with large-scale convective stratification in the ASL. The impact on the results of the sea-ice – mixed-layer model was positive, as far as they could be verified by observations.

The orders of magnitude of the boundary-layer variables seemed to be reasonable, too, taking into account that most of the large-scale quantities are difficult to verify. The large-scale stability appeared to be the key variable in this study. However, recent observations (Overland and Guest, 1991; Kottmeier, personal communication) suggest that the stratification of the atmospheric boundary layer depends strongly on the radiative budget, which in wintertime is dominated by the net longwave radiation, which itself is highly correlated with the presence of clouds. In the present study, clouds are specified by climatological, annual mean and zonally averaged estimates (see Stössel et al., 1990). Experiments with a 20 % change in cloudiness showed slight deviations of the ASL quantities with some indications of the interrelationships mentioned above. Further refinements and experiments are clearly needed to analyse such findings. Since over sea-ice areas cloud processes are often highly correlated to boundary-layer processes which themselves are largely determined by the instantaneous sea-ice conditions (Byers and Stringer, 1992), simulations should be extended to include corresponding interactions (Brinkop, 1992).

The present study focused on problems related to the treatment of different relevant scales within a transition zone from one climate component to another, with emphasis on the efforts to couple atmospheric and oceanic models in sea-ice regions. It is suggested that the coupling interface (including sea ice and snow), together with the atmospheric and oceanic boundary layers, should be considered as an integral transition zone between the 'free' media. While the free atmosphere and ocean are characterised mainly by geostrophic balances, the transition zones are dominated by frictional and buoyancy effects, with various interactive exchanges between the different components. If a heterogeneous distribution of two such components is encountered within one model-grid spacing, the interactions are largely determined by local processes. As indicated in this paper, it is essential to incorporate these sub-grid scale processes and to transform them into large-scale quantities in a physically reasonable way in order to provide a proper transition to the 'undisturbed' bulk of the atmosphere and the ocean.

Although applied here for forced experiments only, a scheme similar to the one presented here is proposed as a tool for matching the GCM-scale coupling over sea-ice covered regions in a more physical way than has been done so far. Together with the implementation of physically more sophisticated sea-ice models in GCMs, this could lead to significant improvements of GCM results in polar regions and lend more credibility to the sensitivity of sea-ice related impacts.

Acknowledgements

We like to thank K.Herterich for valuable discussions on the concept of sub-grid scale parameterisation, K.Hasselmann, L.Bengtsson, P.Lemke and E.Roeckner for valuable comments on the manuscript, M.Grunert and N.Noreiks for finishing the drafts, and P.Besemann and S.Beddig for English review. The Deutsche Wetterdienst (DWD), Offenbach, provided the ECMWF data, which were preprocessed by R.Schnur. This work was mainly sponsored by the Deutsche Forschungsgemeinschaft (DFG) via the Sonderforschungsbereich (SFB) 318.

References

Andreas, E.L., Tucker, W.B. and Ackley, S.F. 1984. Atmospheric boundary-layer modification, drag coefficient, and surface heat flux in the Antarctic marginal ice zone. *J.geophys.Res. 89*, 649-661.

Arya, S. P. S. 1975. A drag partition theory for determining the large-scale roughness parameter and wind stress on the Arctic pack ice. *J. geophys. Res. 80*, 3447-3454.

Banke, E.G., Smith, S.D. and Anderson, R.J. 1980. Drag coefficients at AIDJEX from sonic anemometer measurements. In *Sea ice processes and models* (ed.: R.S.Pritchard). Seattle/USA: University of Washington Press, 430-442.

Beljaars, A.C.M. 1982. The derivation fluxes from profiles in perturbed areas. *Boundary-Layer Meteorol. 24*, 35-55.

Beljaars, A.C.M. and Holtslag, A.A.M. 1991. Flux parameterization over land surfaces for atmospheric models. *J. Appl. Meteorol. 30*, 327-341.

Brinkop, S. 1992. Parameterisierung von Grenzschichtwolken für Zirkulationsmodelle. *Ber.aus dem ZMK, Reihe A: Meteorologie, Nr.2.* Hamburg/Germany: Universität Hamburg.

Businger, J. A., Wyngaard, J. C., Izumi, Y. and Bradley, E. F. 1971. Flux profile relationships in the atmospheric surface layer. *J. atmos. Sci. 28*, 181-189.

Byers, C.A. and W.J.Stringer 1992. Unusual cloud forms in the Arctic winter boundary layer. In: *Third conference polar meteorology and oceanography.* Boston/USA: American Meteorological Society, 7-10.

Claussen, M. 1991a. Local advection processes in the surface layer of the marginal ice zone. *Boundary-layer met. 54*, 1-27.

Claussen, M. 1991b. Estimation of areally-averaged surface fluxes. *Boundary-layer met. 54*, 387-410.

Claussen, M. 1992. Scale aggregation in semi-smooth flow. *Report No. 87.* Hamburg/Germany: Max-Planck-Institut für Meteorologie.

Cubasch, U., Hasselmann, K., Höck, H., Maier-Reimer, E., Mikolajewicz, U., Santer, B.D. and Sausen, R. 1992. Time-dependent greenhouse warming computations with a coupled ocean-atmosphere model. *Climate Dynamics*, in press.

Francis, J.A. 1992. Improvements to TOVS retreivals over sea ice and their application to estimating Arctic energy fluxes. In: *Third conference polar meteorology and oceanography.* Boston/USA: American Meteorological Society, 25-28.

Gordon, A. L. und Huber, B. A. 1990. Southern Ocean winter mixed layer. *J. geophys. Res. 95*, 11655-11672.

Gow, A.J., Ackley, S.F., Buck, K.R. and Golden, K.M. 1987. Physical and structural characteristics of Weddell Sea pack ice. *Rep. No. 87-14.* Hanover/USA: U.S. Army, CRREL.

Hanssen-Bauer, I. und Gjessing, Y. T. 1988. Observations and model calculations of aerodynamic drag on sea ice in the Fram strait. *Tellus 40 A*, 151-161.

Hartmann, J., Kottmeier, C. and Wamser, C. 1992. Radiation and eddy flux experiment 1991 (REFLEX I). *Rep. on Polar Research 105.* Bremerhaven/Germany: Alfred-Wegener-Institut für Polar- und Meeresforschung.

IPCC (Intergovernmental Panel on Climate Change) 1990. *Climate Change: The IPCC scientific assessment.* (eds.: Houghton, J.T., Jenkins, G.J. and Ephraums, J.J.). WMO/UNEP. Cambridge/UK: Cambridge University Press.

Lange, M.A. and Eicken, H. 1991. The sea ice thickness distribution in the northwestern Weddell Sea. *J. geophys. Res. 96*, 4821-4837.

Lemke, P., Owens, W. B. and Hibler, III, W. D. 1990. A coupled sea ice – mixed layer – pycnocline model for the Weddell Sea. *J. geophys. Res. 95,* 9513-9525.

Leppäranta, M. 1983. A growth model for black ice, snow ice and snow thickness in subarctic basins. *Nordic Hydrol. 14*, 59-70.

Louis, J. F. 1979. A parametric model of vertical eddy fluxes in the atmosphere. *Boundary-layer met. 17,* 187-202.

Manabe, S., Spelman, M.J. and Stouffer, R.J. 1992. Transient responses of a coupled ocean-atmosphere model to gradual changes of atmospheric CO_2. Part II: seasonal response. *J. Climate 5*, 105-126.

Marshall, K. 1971. Drag measurements in roughness arrays of varying density and distribution. *Agr. Meteorol. 8*, 269-292.

Martinson, D. G. 1990. Evolution of the Southern Ocean winter mixed layer and sea ice: open ocean deepwater formation and ventilation. *J. geophys. Res. 95,* 11641-11654.

Maykut, G.A. 1986. The surface heat and mass balance. *NATO ASI Series B 146*, 395-464.

McBean, G. 1986. The atmospheric boundary layer. *NATO ASI Series B 146*, 283-338.

Meehl, G. A. and Washington, W. M. 1990. CO_2 climate sensitivity and snow - sea ice albedo parameterisation in an atmospheric GCM coupled to a mixed-layer ocean model. *Clim. Change 6,* 283-306.

Overland, J. E. 1985. Atmospheric boundary layer structure and drag coefficent over sea ice. *J. geophys. Res. 90*, 9029-9049.

Overland, J.E. and Guest, P.S. 1991. The Arctic snow and air temperature budget over sea ice during winter. *J. Geophys. Res. 96*, 4651-4662.

Overland, J.E. and Davidson, K.L. 1992. Geostrophic drag coefficient over sea ice. *Tellus 44A*, 54-66.

Owens, W. B. and Lemke, P. 1990. Sensitivity studies with a sea ice – mixed layer – pycnocline model in the Weddell Sea. *J. geophys. Res. 95,* 9527-9538.

Simmonds, I. and Budd, W.F. 1991. Sensitivity of the southern hemisphere circulation to leads in the Antarctic pack ice. *Q.J.R. Meteorol. Soc. 117*, 1003-1024.

Stössel, A. 1985. Thermodynamic calculations of ice production in the northern Baltic proper. *Dt. hydrogr. Z. 38*, 261-284.

Stössel, A. 1991. Southern Ocean sea-ice simulations forced with operationally derived atmospheric analyses data. *Report No.65*. Hamburg/Germany: Max-Planck-Institut für Meteorologie.

Stössel, A. 1992. Sensitivity of Southern Ocean sea-ice simulations to different atmospheric forcing algorithms. *Tellus*, in press.

Stössel, A., Lemke, P. and Owens, W. B. 1990. Coupled sea ice – mixed layer simulations for the Southern Ocean. *J. geophys. Res. 95*, 9539-9555.

Trenberth, K.E. and Olson, J. G. 1988. ECMWF global analyses 1979 - 1986: circulation statistics and data evaluation. *Technical note TN-300 + STR.* Boulder/USA: NCAR.

Wadhams, P., Lange, M. A. and Ackley, S. F. 1987. The ice thickness distribution across the Atlantic sector of the Antarctic Ocean in midwinter. *J. geophys. Res. 92*, 14535-14552.

Walter, B. and Overland, J.E. 1991. Aircraft observations of the mean and turbulent structure of the atmospheric boundary layer during spring in the Central Arctic. *J. geophys. Res. 96*, 4663-4673.

Worby, A. P. and Allison, I. 1991. Ocean – atmosphere energy exchange over thin, variable concentration Antartic pack ice. *Ann. Glaciol. 15*, 184-190.